International Journal of Applied Earth Observation and Geoinformation 57 (2016) 49–60

Contents lists available at ScienceDirect

International Journal of Applied Earth Observation and Geoinformation

journal homepage: www.elsevier.com/locate/jag

Enhanced change detection index for disaster response, recovery assessment and monitoring of accessibility and open spaces (camp sites)

Dilkushi A. de Alwis Pitts*, Emily So

Department of Architecture, University of Cambridge, United Kingdom

Enhanced Change Detection Index for Disaster Response, Recovery Assessment and Monitoring of Accessibility and Open Spaces (Camp Sites)

Authors

Dilkushi A. de Alwis Pitts[a], Emily So[a]

[a]Department of Architecture, University of Cambridge, United Kingdom

email: kad49@cam.ac.uk

Abstract The availability of Very High Resolution (VHR) optical sensors and a growing image archive that is frequently updated, allows the use of change detection in post-disaster recovery and monitoring for robust and rapid results. The proposed semi-automated GIS object-based method uses readily available pre-disaster GIS data and adds existing knowledge into the processing to enhance change detection. It also allows targeting specific types of changes pertaining to similar man-made objects. This change detection method is based on pre/post normalized index, gradient of intensity, texture and edge similarity filters within the object and a set of training data. Once the change is quantified, based on training data, the method can be used automatically to detect change in order to observe recovery over time in large areas. Analysis over time can also contribute to obtaining a full

picture of the recovery and development after disaster, thereby giving managers a better understanding of productive management practices.

Keywords: Change Detection, Remote Sensing, Disaster Response and Recovery, Roads, Open Spaces

1. Introduction

Rapid and robust impact assessment of poorly-accessible affected areas is essential for initiating effective emergency response actions following disasters (Dell'Acqua et al. 2009), especially in highly populated urban areas (Vu and Ban 2010). Information pertaining to accessibility is critical in order to organize medical help and evacuation as well as aiding in both early- and long-term recovery evaluation (Joyce et al. 2013). In addition, identifying the location and sizes of open spaces is important in the early phases of emergency response. This information allows emergency managers to select the best plots for camps. These campsites also require monitoring and evaluation during in early-recovery phase to understand the population's re-housing.

Information on damage caused by an event can be derived quickly from suitable very high-resolution (VHR) satellite imagery (Walter, 2004) by comparing data from a chosen reference before the event (pre-event) to imagery acquired shortly after the event (post-event). The availability of pre- and post-event data opens the possibility for gathering impact assessment data using change detection in complex environments such as urban areas. Change detection from high spatial-resolution images such as IKONOS and QuickBird is even more challenging, especially in complex environments characterised by small objects such as houses, individual trees and roads, and by shadows (Pagot et al., 2008).

In general, change detection techniques can be grouped into two types: pixel-based and object-based (Blaschke 2010, Chen et al., 2012). Pixel-based change detection analysis refers to using a change detection algorithm to compare the multi-temporal images pixel-by-pixel while object-based change detection analysis refers to using a change detection algorithm to compare multi-temporal images object-by-object. However, the definition of pixel-based and object-based change detection is not absolute. The most basic feature of object-based approaches is to segment the image and regard the objects as the basic unit of operation, rather than the pixel-based approach, which regards a single pixel as the basic unit (Dai, et al., 1998).

Object-based methods have the potential to provide more accurate results than traditional pixel-based methods (Al-Khudhairy et al. 2005), but choosing the object feature is not straightforward because the

high information content of VHR images requires an accurate definition of the object. Thus the object detection step causes most of the error (Michaelsen et al. 2006).

Most object-based algorithms concentrate on detecting objects such as rectangular buildings (Lin et al. 1998) or parallel lines for detecting roads. This search is complex and rarely accurate, especially after disasters. As noted in the related literature, road extraction has been achieved in single or multiple operations such as image segmentation (Yang and Wang 2007, Singh et al. 2014), classification (Mohammadzadeh et al. 2008), using morphological operations (Mena and Malpica 2005, Al-Khudhairy et al. 2005) and merging relevant road segments (Akcay and Aksoy 2008, Mohammadzadeh, 2009). Hough transform and edge detection have also been used to detect linear parallel segments with constant width (Talib and Ramli 2015), snakes (Butenuth and Heipke 2010) (contour-based object outlines) and matching road templates to obtain networks (Touya 2010). Hiremath et al., 2010 have used a sequence of filtering followed by segmentation, grouping and optimization on VHR images to identify open spaces in complex urban environments.

Many current change-detection mechanisms do not make effective use of available pre-disaster data and existing knowledge. Hence using pre-disaster GIS objects such as roads, open spaces, bridges etc. as indicators allows targeting the search for specific changes to these areas within the objects of interest. The proposed indicator-specific method uses readily available pre-disaster GIS data and existing knowledge to enhance the detection of change while offering the possibility to target specific types of changes pertaining to similar man-made objects.

The GIS object-based method discussed here is based on a pre/post normalized index, gradient. texture, and edge similarity filters within the object and an existing set of training data. The proposed semi-automated method is evaluated with QuickBird, Geoeye 1, and Worldview 2 datasets for abrupt changes soon after a disaster. The method could also be automated to monitor progressive changes months after a disaster.

2. Method

2.1. Case Study Sites

2.1.1. Van, Turkey

The Van earthquake was a destructive M7.1 earthquake that struck the city of Van in eastern Turkey on Sunday, 23 October 2011 at 13:41 local time. Based on the reports at least 534 people were killed, 2,300 injured and 14,618 buildings and homes destroyed or damaged in the Ercis-Tabanli-Van area (Earthquake.usgs.gov 2015). As a part of the SENSUM (European Commission under FP7 (Seventh Framework Programme): SENSUM: Framework to Integrate Space-based and in-situ sENSing for

dynamic vUlnerability and recovery Monitoring, 312972) project, the Van earthquake was selected for study because it was one of the most recent destructive, vast earthquakes for which imagery was available and suitable for a data-poor country for which remotely sensed tools were well suited.

Table 1 Satellite Data for Van, Turkey

Imagery	Acquisition Date
Pre- disaster (WV02)	06th May 2011 - 5 months before earthquake
Post disaster 1 (Geoeye-1)	12th Jan 2012 - 2.5 months after earthquake
Post disaster 2 (Geoeye-1)	22nd Feb 2012 - 3 months after earthquake
Post disaster 3(WV02)	05th June 2013 - 1 year and 7 months after earthquake

The WV02 (WorldView-2) sensor provides a high-resolution Panchromatic band and 8 multispectral bands: 4 standard colors – (red(630 -690 nm), green (510 - 580 nm), blue (450 - 510 nm), and near-infrared 1(770 - 895 nm) –and 4 new bands (coastal, yellow, red edge, and near-infrared 2). For this study we used only 4 spectral bands out of the 8 bands, omitting 4 new bands. The resolution of the Panchromatic (nominal at nadir) is 0.46 m and multispectral (nominal at nadir) is 1.85 m. The Geoeye-1 has a Panchromatic band (450 - 800 nm) and 4 multispectral bands, blue (450 - 510 nm), green (510 - 580 nm), red (655 - 690 nm) and near infrared (780 - 920 nm). The resolution of the Panchromatic (nominal at nadir) is 0.41 m and multispectral (nominal at nadir) is 1.65 m.

2.1.2. Muzzaffarabad, Pakistan

The Kashmir earthquake was a destructive 7.6 Mw earthquake that struck the northwest region of Pakistan, near the city of Muzaffarabad, on 8 October 2005 at 08:52 local time (USGS, 2015).

The Muzaffarabad area was selected as a study site of the ReBuilDD (Remote sensing for Built environment Disaster and Development) (Brown etal.2012) project because it was a major earthquake with severe damage. The timing, the extent of the disaster and the fact that very little ground based data existed, made it a well suited as a case study of remotely sensed data.

Table 2 Imagery and Data Acquisition dates for Muzzaffarabad, Pakistan

Imagery	Acquisition Date
Pre-disaster (QuickBird)*	13th August 2004 – 14 months before earthquake

Post disaster 1 (QuickBird) *	22nd October 2005 – 2 weeks after earthquake
Post disaster 2 (QuickBird) *	13th June 2006 – 8 months after earthquake

*QuickBird-2 imagery contained five bands namely Blue (450 - 520 nm), Green (520 - 600 nm), Red (630 - 690 nm), NIR (760 - 900 nm), and PAN (760 - 850 nm). The spectral bands have a resolution of 2.44 m and the PAN band has a pixel resolution of 0.61 m nominal at nadir.

2.2. Data Acquisition and Data Preparation

The process of initial data preparation for the proposed change detection method is shown in Figure 1. The following paragraphs explain the data preparation in detail.

OpenStreetMap data: The data pertaining to the road layer was downloaded directly from the OpenStreetMap (OSM) archive (GEOFABRIK (Download.geofabrik.de)). In the case of Muzzaffarabad, the street layers for the primary and secondary roads were manually digitised from the QuickBird VHR images using QGIS since the OSM data were incomplete.

Satellite Images: For the case study of Van, four satellite images were acquired from 2011 to 2013 (Table 1). For the case study of Muzzaffarabad, three satellite images were acquired from 2004 to 2006 (Table 2).

Geo-rectifying the pre-disaster image: All the satellite data were co-registered to the road layers obtained from OSM to ensure the best alignment (accuracy <1.47m). The pre-disaster IR R,G bands were first PAN-sharpened (using QGIS OTB (OrfeoToolBox) Processing toolbox) and then co-registered to the reference vector layer such as a road layer (See Figure 1).

Geo-rectifying the post-disaster image: The PAN-sharpened post-disaster image was geo-rectified using buildings, roads, and junctions identified in both the pre and post images and used as ground control points.

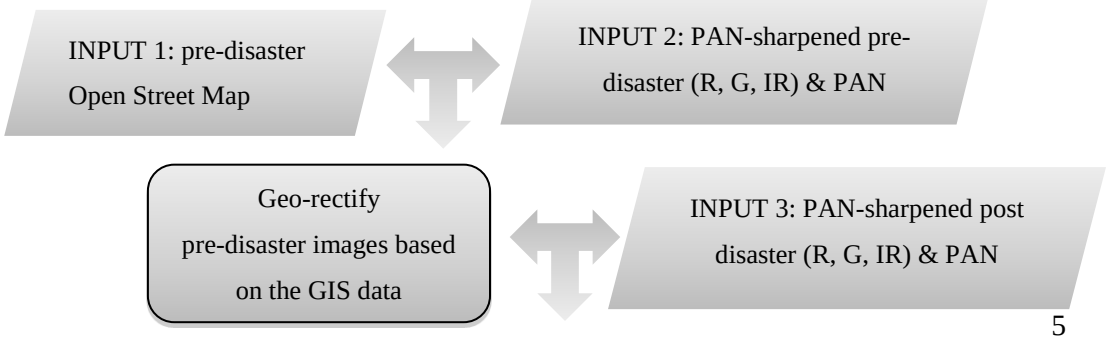

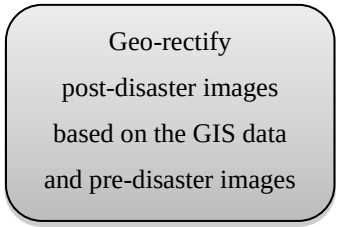

Figure 1 Data preparation workflow: Pre-disaster images are PAN-sharpened and geo-rectified to the Open Street Map and then the PAN-sharpened post-disaster images are geo-rectified to the pre-disaster images.

2.3. Accessibility: Building and Buffering Road Data

Before using the road layer in the accessibility workflow Figure 2, the road polylines were merged and then split into 100-meter long segments. From visual inspection for Van, it was decided to apply a 6-meter buffer and a 4-meter buffer to represent primary and secondary roads respectively. For Muzzaffarabad a buffer distance of 4 meters and 2 meters for primary and secondary roads was identified. As seen in workflow Figure 2, each of the 100m segments was buffered and then clipped for the complete time series, thus creating the multi-temporal set of raster road segments, which are the input of the change detection index shown in Figure 3.

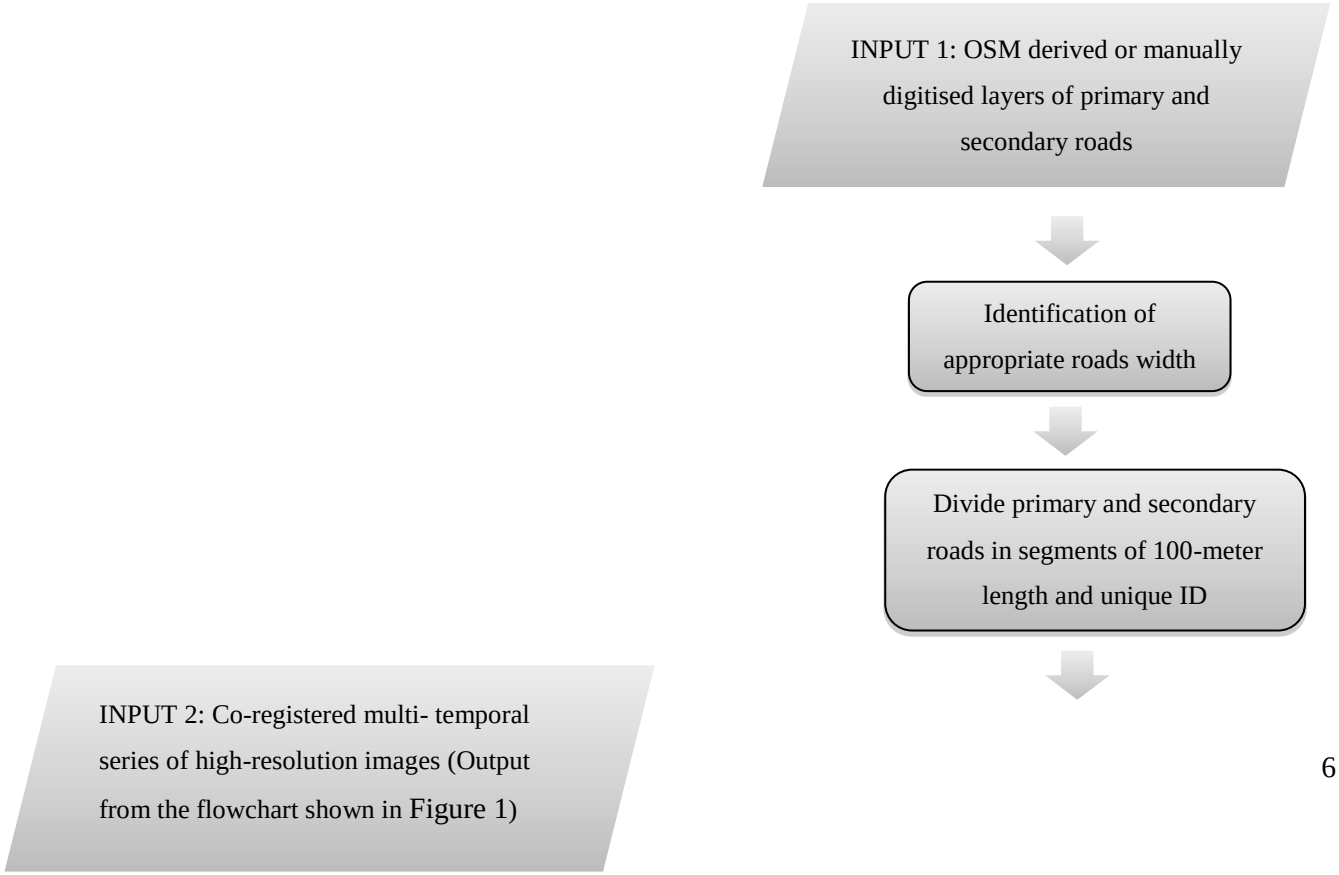

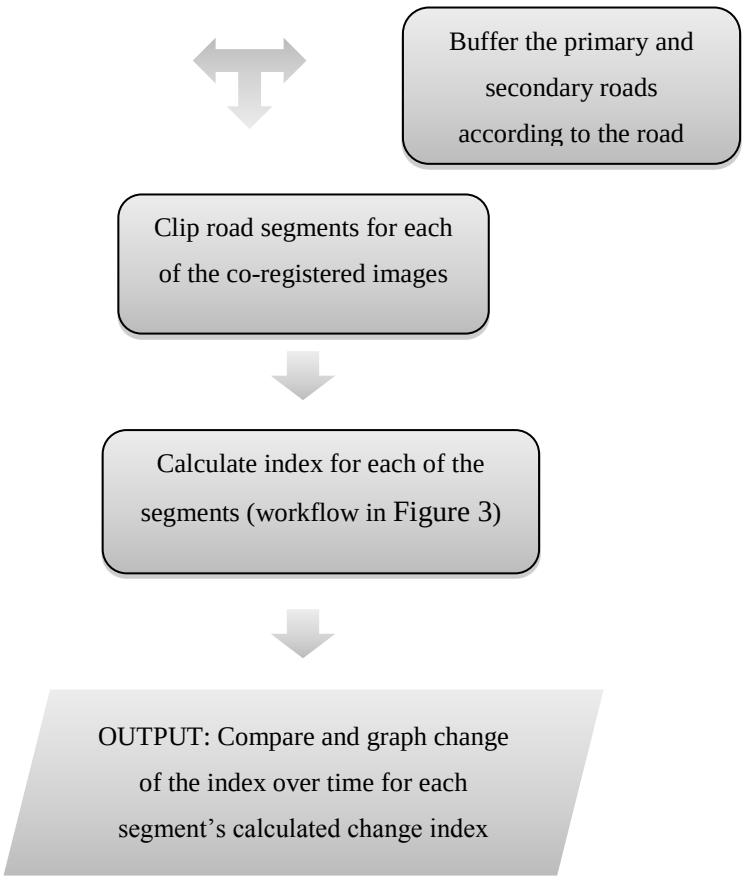

Figure 2: The workflow for accessibility showing how the roads (GIS layers) are buffered and used to clip the pre- and post-images and prepare to calculate the Enhanced Change Detection Index

2.3.1. Pre-Post Normalized Difference of the Satellite data

As per workflow in Figure 3 the pre-post normalized difference between the PAN-sharpened, geo-referenced bands (R, G, IR) and PAN bands is calculated using Equation 1 for each road segment. The pre-post normalized difference removes changes in reflectance due to acquisition times within the day. The normalized ratio in the denominator of Equation 1 helps to compensate for differences both in illumination within an image due to slope and aspect, and differences between images due to time of day or season when the images were acquired. Taking the square root is intended to correct values approximate a Poisson distribution and introduce a normal distribution, producing a linear measurement scale. Adding a constant of 0.5 to all pre-post normalized values does not always eliminate all negative values, but it leaves fewer of them.

$$\frac{(\frac{POST-PRE}{POST+PRE}+0.5)}{|(\frac{POST-PRE}{POST+PRE}+0.5)|} . \sqrt{|(\frac{POST-PRE}{POST+PRE} + 0.5)|} \quad \text{Equation 1}$$

2.3.2. Enhanced Change Detection Index for Roads

As shown in Figure 3 each normalized difference of PAN and PAN-sharpened (IR, R, G) bands for each road segment was subjected to Vigra edge detection in QGIS (QGIS Development Team,

2015) and texture using GDAL's (QGIS) roughness parameter. Edges and texture filters of the pre-post normalized images were used to capture object specific changes in edges. Next the gradient is calculated for each object in pre- and post-images PAN sharpened bands (R, G, IR) and PAN bands and then normalized (for each band) using Equation 1. The change of edges, texture and gradient parameters are calculated within each of the objects as per the flowchart in Figure 3 (accessibility). This creates 12 change-related parameters (4 pertaining to edges, 4 to texture, and 4 to the gradient) for each object in regard to accessibility (road segments).

2.3.3. Visual Index (Training Data) for Road Segments

A visual index (VI) is developed by comparing the pre and post images visually in a way that is analogous to a linear visual scale for change. This VI, in the range between 0 and 10 documents the changes as perceived by a human. As shown in

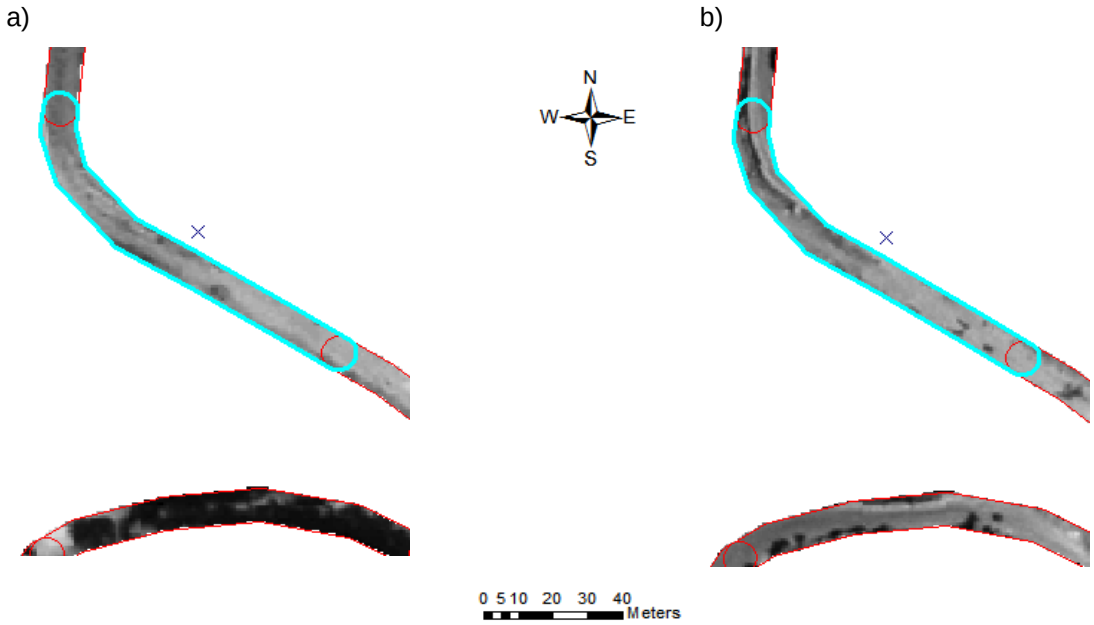

c) d)

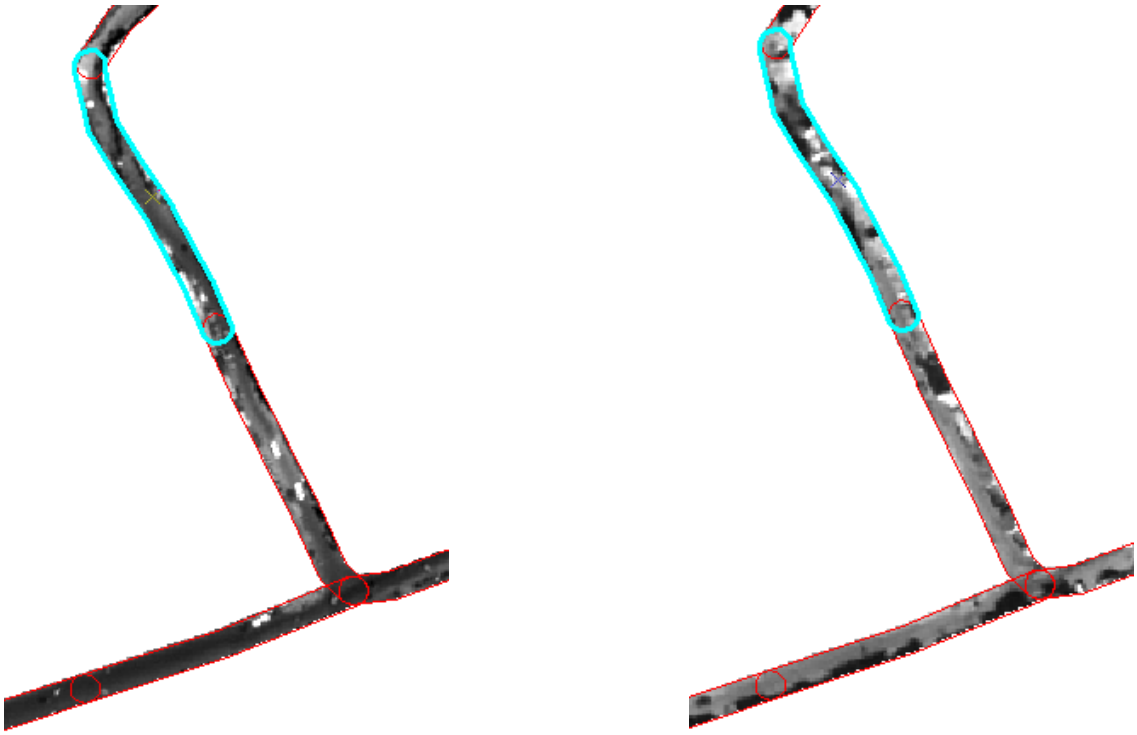

Figure 4, pre and post images of road segments (objects) of about 1/10 of the total road segments were used visually to determine the VI. The segments that had mild changes were assigned a small VI (close to 0, Figure 4 a) and b)) and the segments that showed large changes were assigned large VI values (close to 10,Figure 4 c) and d)).

Then as seen in Figure 3, this visual index was used as a training set and regressed against the derived values of pre-post normalized gradient, edges, and roughness of each road segment.

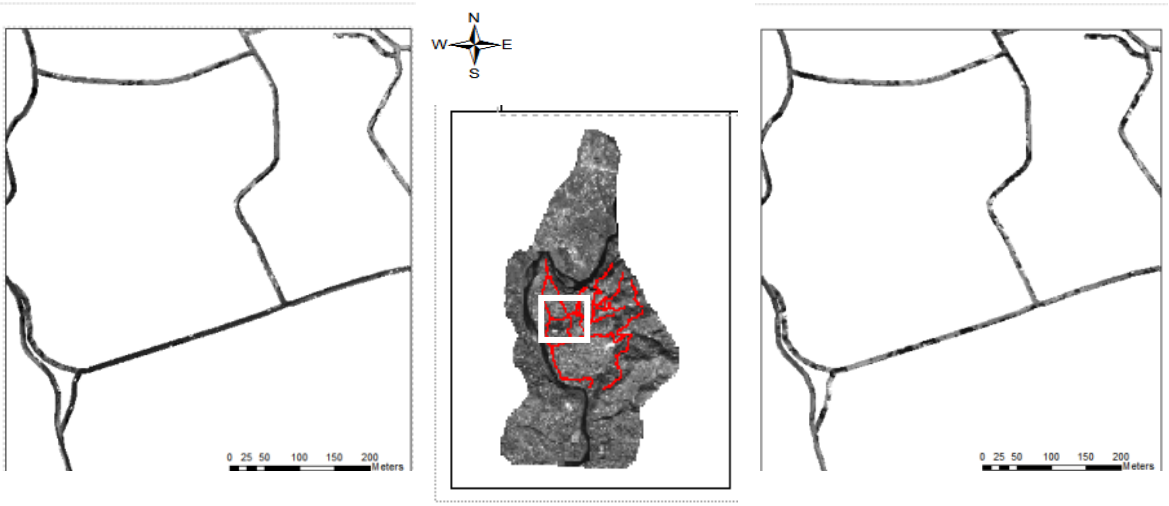

INPUT I: Road segments of the co-registered pre-disaster image

INPUT 2: Road segments of the co-registered post-disaster image

Calculate the gradient of pre- and post-images

Normalized road segments pertaining to the co-registered pre-disaster and post-disaster image using Equation 1

Normalized road segments pertaining to the co-registered pre-disaster and post-disaster image using Equation 1

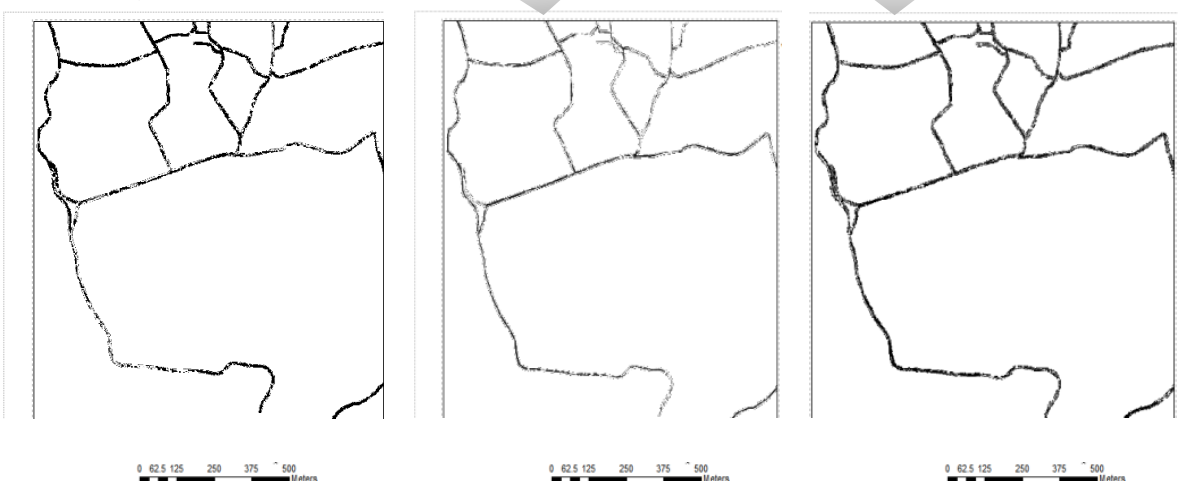

Index pertaining to the roughness of the normalized image

Index pertaining to the edges of the normalized image

Normalized index pertaining to the gradient of pre- and post-disaster images

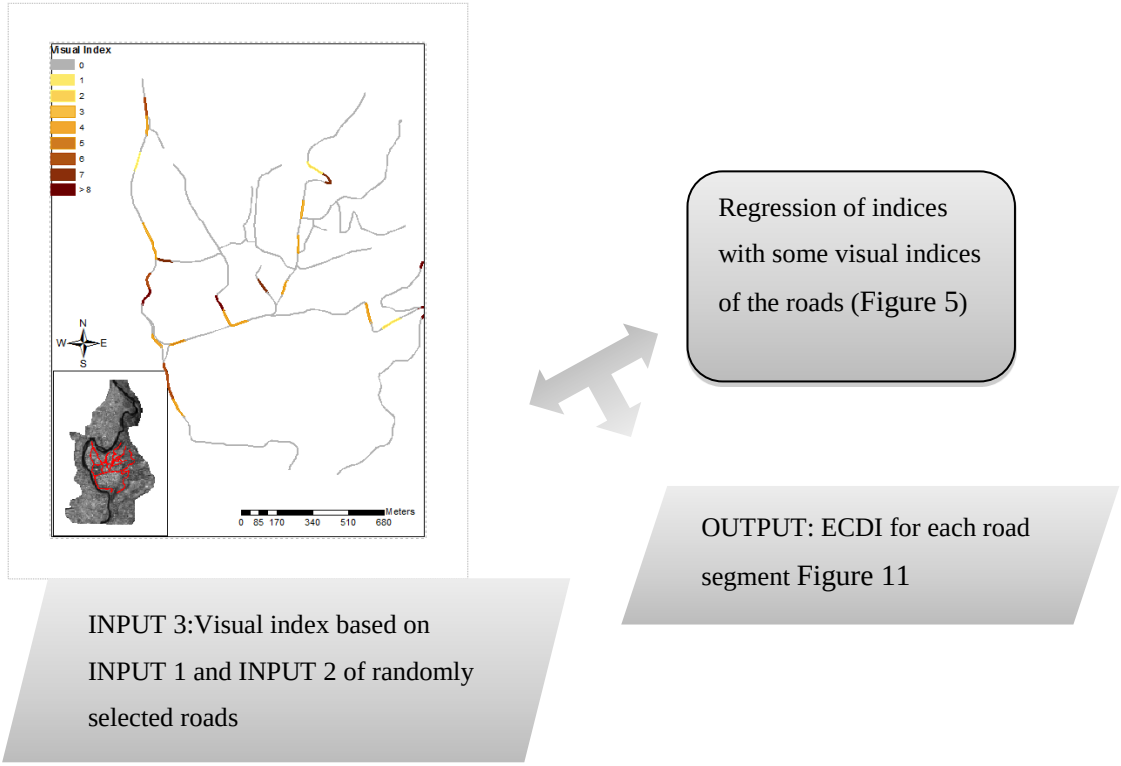

Figure 3: Workflow showing the enhanced change detection index (ECDI) for the roads in Muzzaffarabad. The pre- and post-disaster images (outputs from the workflow shown in Figure 2) are normalized and a value pertaining to the roughness and edges are calculated for each road segment. The gradient is calculated for each road segment in each for the pre- and post-disaster images individually and then normalized (Equation 1). The change-related parameters for each road segment are then regressed with the visual index to find the coefficients to create the ECDI.

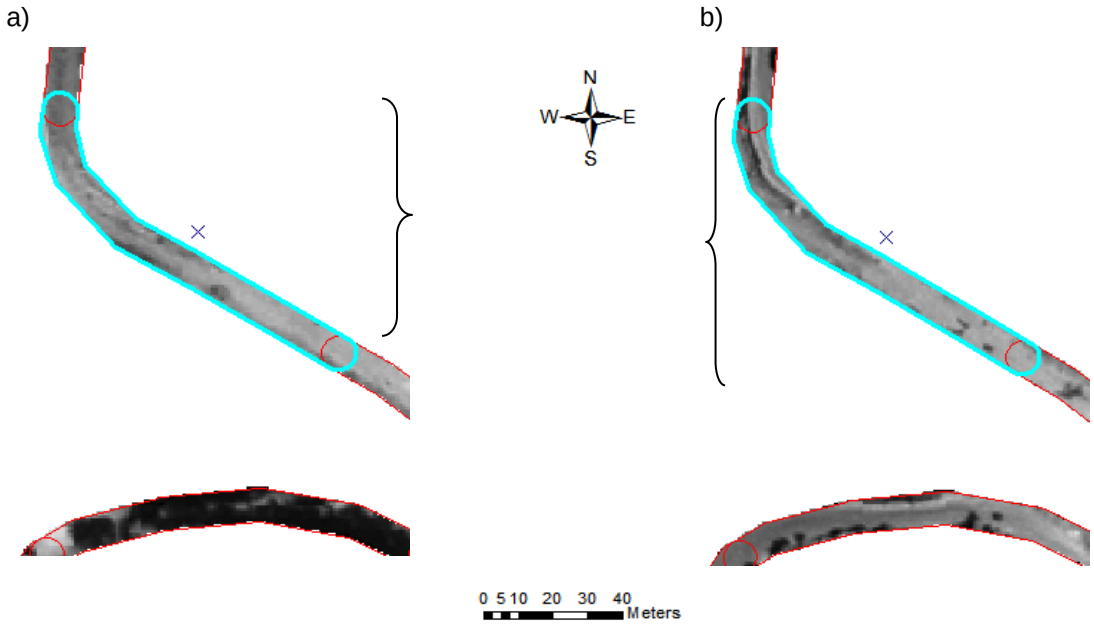

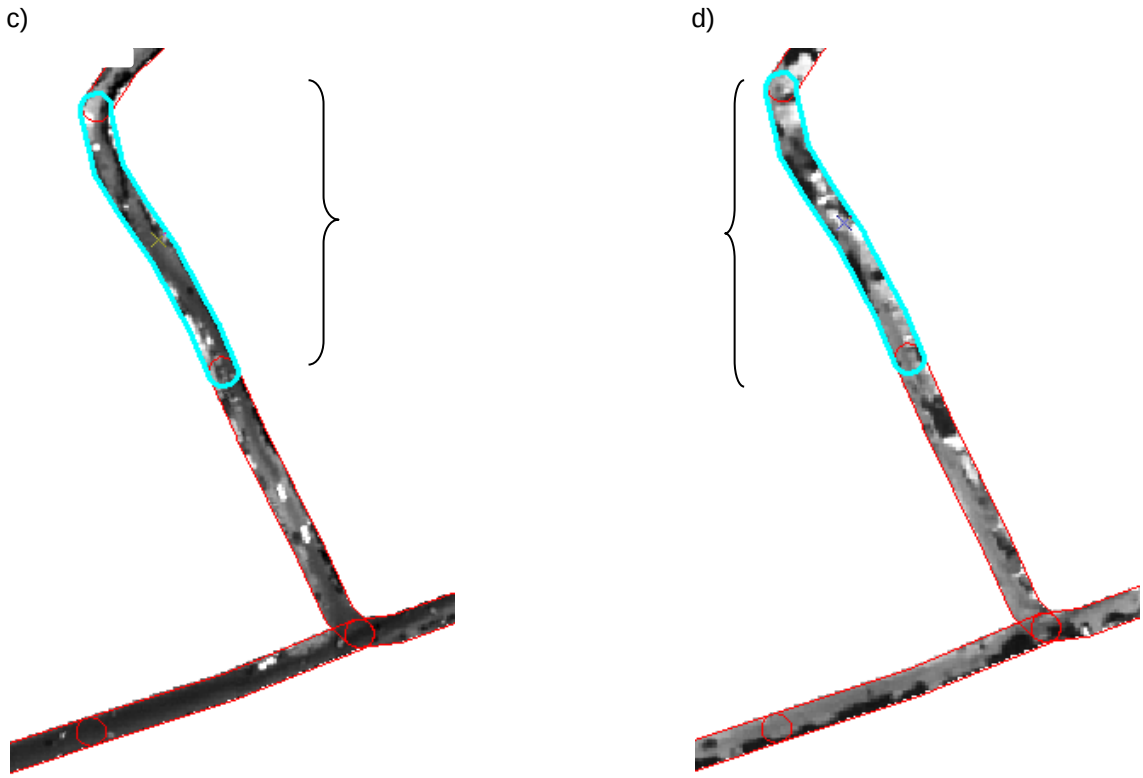

Figure 4 a) and b) are the pre- and post-images of the clipped roads. By looking at these images, a visual index of 2 was determined and assigned because the roads have not changed much between the two images. C) and d) show a considerable change, hence a value of 9 is used as the visual index. Thirty road segments were visually analysed and an appropriate visual index determined in Muzzaffarabad.

2.3.4. Regression

The visual index derived by observing the visual changes in pre- and post-disaster images for 30 road segments was regressed with the values obtained from change in texture, gradient, and edges.

PAN_Texture_	PAN_Gradient_	PAN_Edges_	IR_Texture_	IR_Gr
0.221810963	0.530726738	0.09235763	0.2175515	0.5
0.22992012	0.5103156	0.07699201	0.2006765	0.54
0.200479416	0.549637636	0.09600959	0.1956632	0.54
0.235774628	0.489457392	0.10375624	0.166315	0.51
0.152853313	0.550523211	0.11808296	0.1979714	0.52
0.208402731	0.508932503	0.09840798	0.2059248	0.55

Visual_Index
6
6
5
4
4

Figure 5 The calculated normalized texture, gradient and edge values derived for each road object for (R, G, IR) and PAN bands are regressed with the visual index obtained by observing the visual changes in pre- and post-disaster images for 1/10th of the road segments. The obtained regression coefficients are then used to calculate the ECDI (enhanced change detection index) for all the roads.

The R square value was 0.89 with low P values for PAN and PAN-sharpened IR bands derived gradient, texture, and edge parameter. This low P value with a high R square combination indicates that changes in the predictors (gradient, texture, and edge) are related to changes in the response

variable (visual index), thereby indicating that the model explains a great deal of the response variability. Red and green band derived parameters did not contribute significantly. The graph of the visual index *vs*. ECDI is shown in Figure 6.

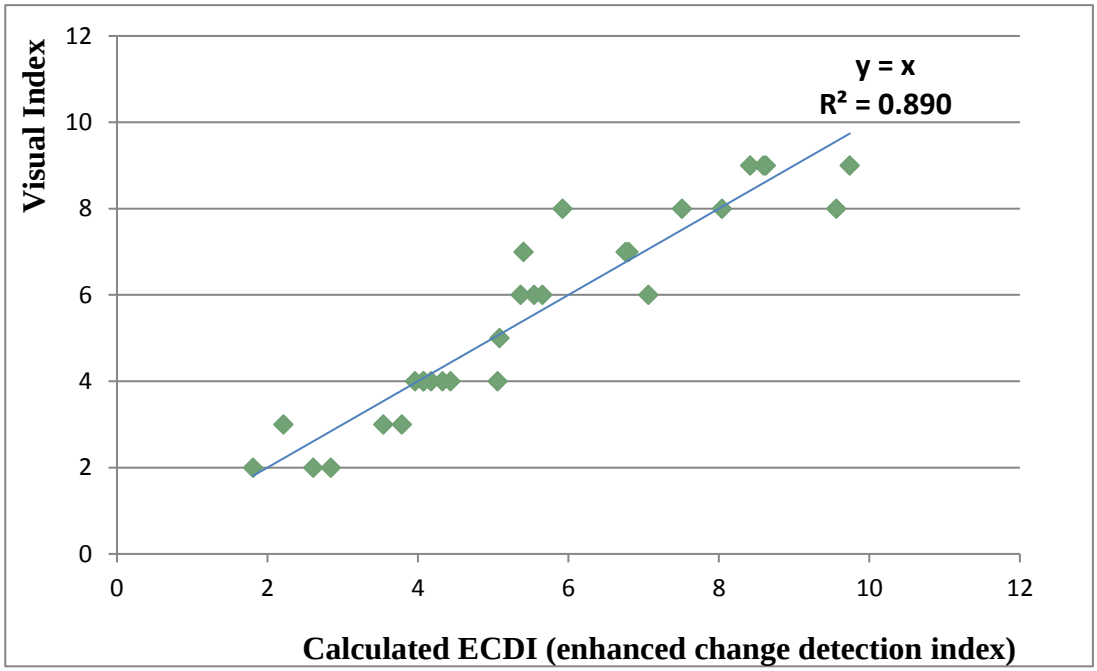

Figure 6: The visual index (using Figure 4) *vs*. the calculated ECDI (enhanced change detection index) (Figure 5) for the selected roads. The figure shows a good correlation between the visual index and the pre- and post-disaster normalized parameters (texture, edges, and gradient) used to create ECDI.

2.4. Open Spaces

The open spaces were detected by segmenting the pre-disaster panchromatic sharpened green image using a Meanshift segmentation algorithm (see the workflow in Figure 7). Camp sites mostly within 2km from the main roads and within areas 10,000 and 50,000 m^2 in Van and Muzaffarabad were selected as probable camp-sites. Each selected polygon was used to clip the open space off the pre- and post-event panchromatic and PAN (panchromatic)-sharpened images. The same rationale applied in the accessibility workflow was used for open spaces. The workflow shown in Figure 7 was used to detect local changes.

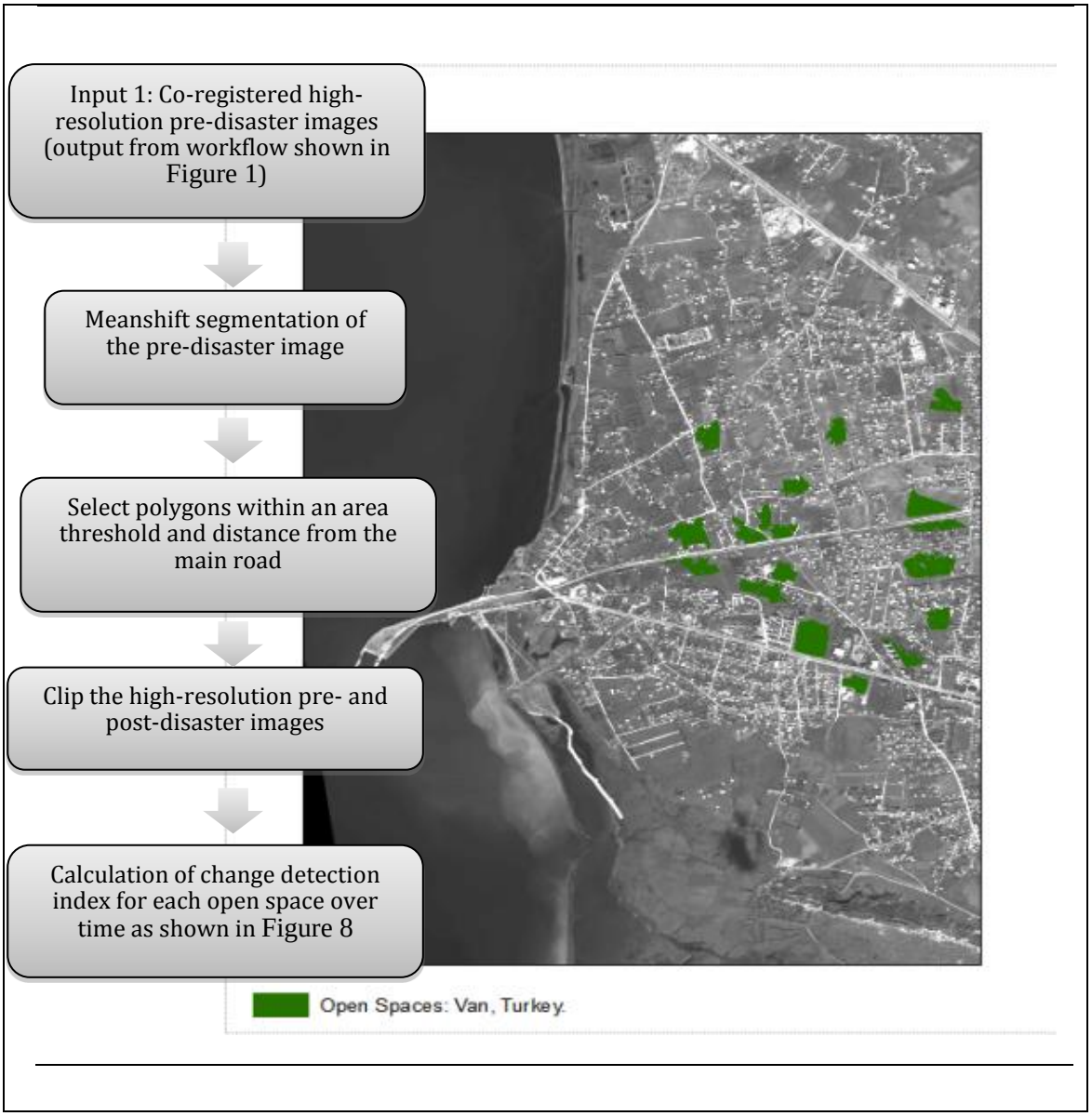

Figure 7: Workflow for open spaces. Co-registered high-resolution pre-disaster images are segmented using the mean shift on the Green band to select homogeneous regions. Then an area threshold and a distance from the main roads are assigned to select the most suitable and accessible open spaces for campsites. The thresholds vary in the two case studies.

2.4.1. Enhanced Change Detection Index (ECDI) for Open Spaces

As shown in Figure 8 the ECDI for each open space was calculated similarly to the road segments by first obtaining the normalized difference between the PAN-sharpened, geo-referenced pre- and post-disaster images (bands PAN, and PAN-sharpened IR, Red, and Green) using Equation 1. Similar to the road segments, the images were subjected to a texture (roughness filter) and edge extraction (Vigra edge). Each open space area segment was assigned a number based on the texture/roughness and edge density in all bands. Then the gradient was calculated for each open space segment in the

pre- and post-disaster images. The gradients were then pre/post normalized using Equation 1 to obtain a value for each open space area.

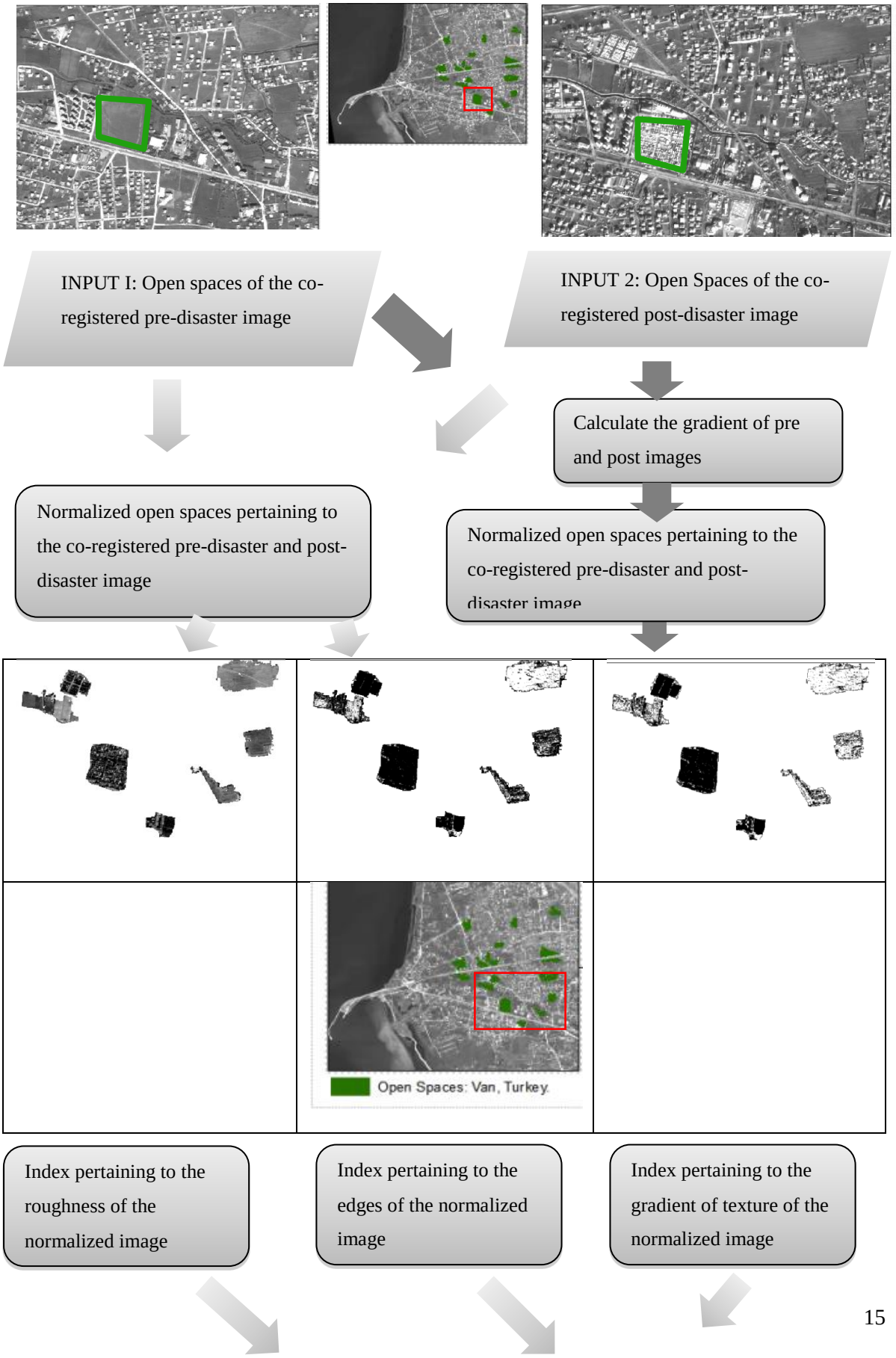

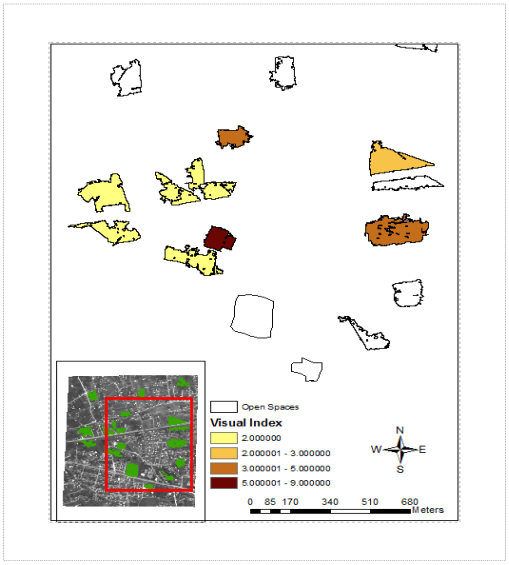

Regression of indices with some visual indices of the open spaces

OUTPUT: ECDI for each open space shown in Figure 12

INPUT 3:Visual Index based on INPUT 1 and INPUT 2 of randomly selected open spaces

Figure 8: The workflow of the change index for open spaces. The flowchart shows how the normalized images are calculated from the pre- and post-disaster images and the texture, gradient, and edge differences within each object, which are used to regress with the visual index of open spaces. The regression coefficients are used to calculate the enhanced change detection index (ECDI) for all the objects.

2.4.2. Visual Index (Training Data) for Open Spaces

Similar to the road segments, for open spaces a visual index (VI) between 0 and 10 is developed by comparing the pre and post images visually in a way that is analogous to a linear visual scale to represent change. As shown in

Figure 9, pre and post images for open spaces (objects) were used to determine the visual change. As for the road segments, the open spaces that had mild changes were assigned a small VI (close to 0,

Figure 9 c) and d)) and the segments that showed large changes were assigned large VI values (close to 10,

Figure 9 a) and b)). Then as seen in Figure 8, this visual index was used as a training set and regressed against the derived values of pre-post normalized gradient, edges, and roughness of each open space.

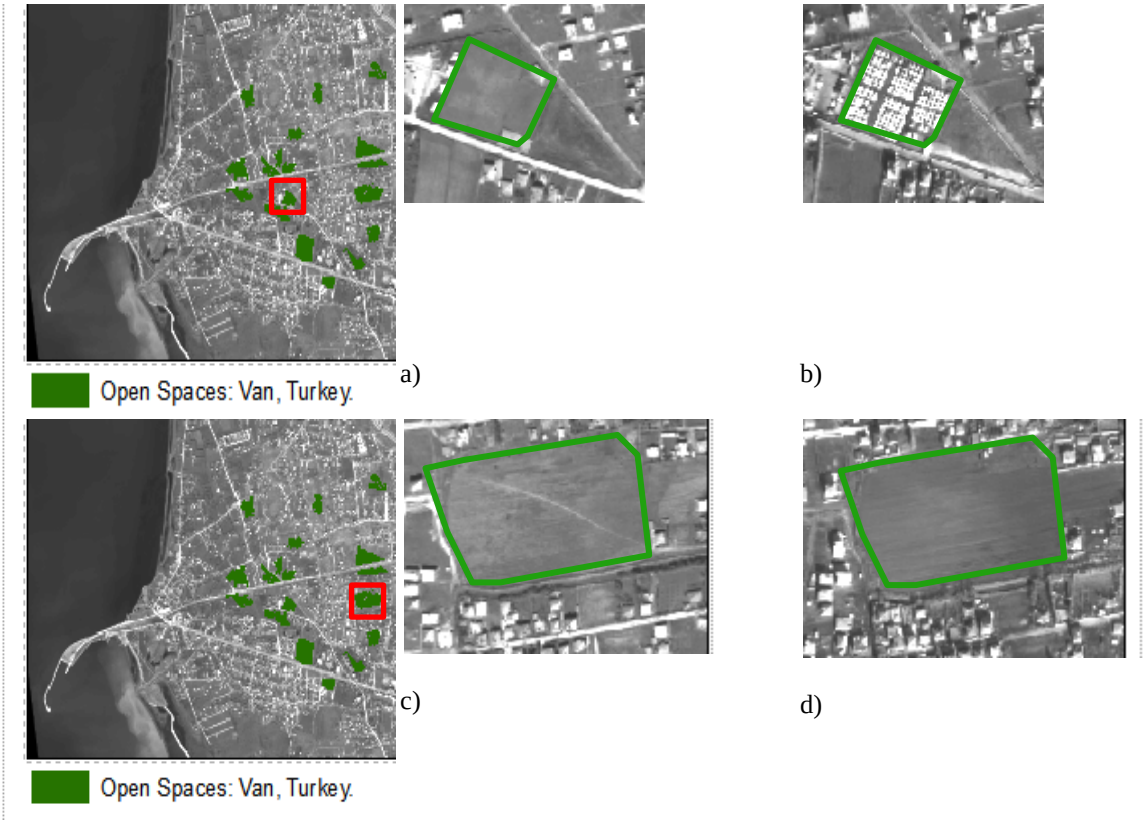

297

298 **Figure 9 a) and b) show the pre- and post-disaster images of an open space occupied as a campsite. C) and d) show**
299 **the pre- and post-disaster images of an open space not occupied by a campsite after disaster. The visual differences**
300 **between the open space are shown in a) and b) is large, so it is given a visual index of 9. The visual difference between**
301 **the open space are shown in c) and d) is relatively small, hence is given a visual index of 3. A visual index smaller than**
302 **3 was not given because there were significant differences in the grass patch between the pre- and post-disaster**
303 **images.**

304

305 **2.4.3. Regression**

306 A methodology similar to that used for roads was utilized for open spaces. Through regression we
307 acquired the coefficients needed to combine the derived pre-post normalized gradient, edge and
308 roughness parameters with the visual perception (VI) to form an ECDI for all the open spaces,
309 especially where the change were ambiguous to quantify visually. The R square value was 1 with low
310 P values for gradient and edge parameters derived from PAN-sharpened IR band .The combination of
311 a low P value with a high R square indicates that changes in the predictors (texture, edges, and
312 gradient changes to the object) are related to changes in the response variable (visual index), so the
313 model explains a great deal of the response variability (visual index). Unlike in roads, PAN-sharpened
314 IR bands show dominance over the PAN for open spaces, particularly those covered in vegetation.
315 Red and Green band derived parameters did not contribute significantly. The graph of visual index
316 vs. ECDI is shown in Figure 10.

317

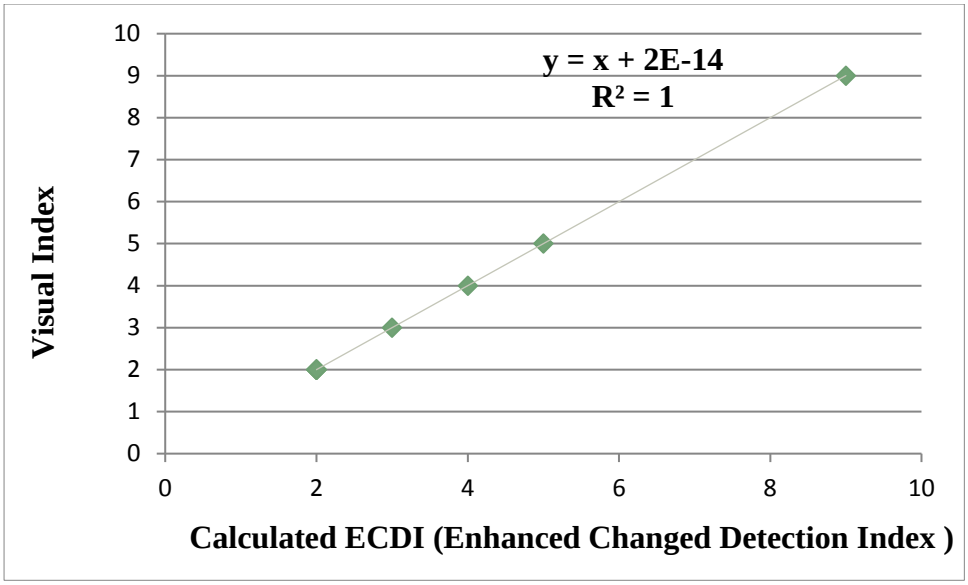

Figure 10: The visual index (as seen in Figure 10) vs. calculated ECDI (

Figure 9) for the selected open spaces. The figure shows a good correlation between the visual index and the pre/post normalized changes in texture, edges, and gradient used to calculate the ECDI.

3. Results

3.1. Accessibility

Figure 11 shows the pre/post normalized relative change (ECDI) for the road network in Muzaffarabad. The higher ECDI indicates a significant change, implying that the roads have changed since the disaster when compared to the pre-disaster image. Knowing if a road segment has changed relative to the other roads can allow emergency vehicles to find an alternative route that has very little change. Because remotely sensed data let us process large areas, alternative routes can be easily found.

As shown in

Table 3, each image can be compared to the pre-disaster image as well as an image immediately following a post-disaster image to get a better picture of the recovery situation.

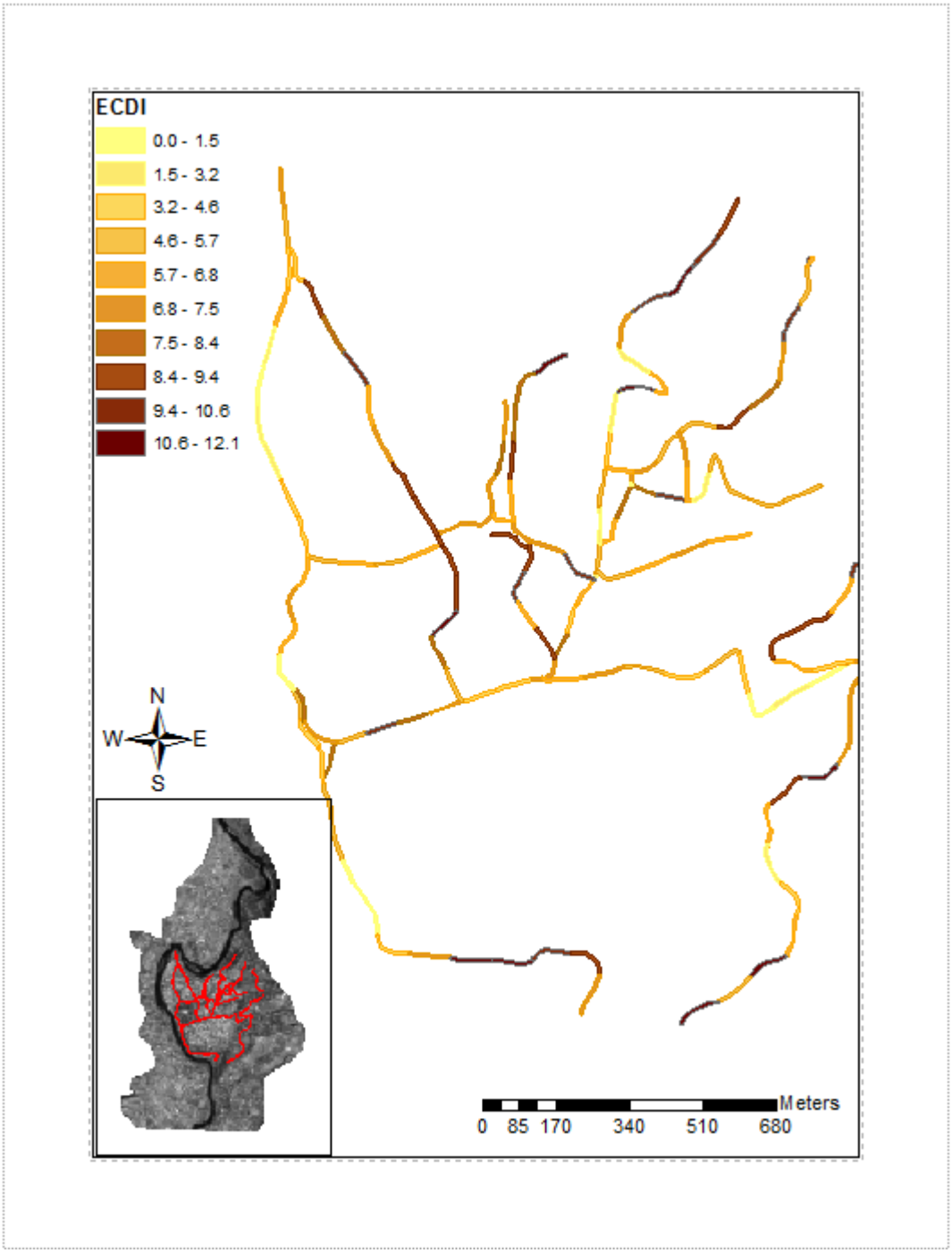

Figure 11: Enhanced change detection index (ECDI) for roads obtained between pre-disaster and post-disaster. Higher indices (represented by darker colors) indicate greater changes after disaster.

Table 3 Accessibility Case Study Scenarios

Table 3 outlines scenarios that can be seen when ECDIs are observed over time. They are obtained by comparing post-disaster images to pre-disaster image.

ECDI of Pre disaster & Post T1*	ECDI of Pre disaster & Post T2*	ECDI of Post T1*& Post T2*	Scenario
>5	<5	>5	Road affected by post T1 date and recovered by Post T2 date
>5	>5	<5	Road affected by post T1 date and NOT recovered by Post T2 date
<5	<5	<5	Road not affected
<5	>5	>5	Road not affected by post T1 data and not modified by Post T2 date

*Post T1 and Post T2 are dates after the disaster.

As seen in

Table 3 the variation of roads affected by the disaster and recovered by the post T1 date and/or post T2 date can be determined. By obtaining the ECDI over time (

Table 3), the condition of roads over time can be used to improve management practices during future scenarios.

3.2. Open Areas

Shown in Figure 12 is the final output of the ECDI of open areas. The higher numbers in the ECDI indicate a major change in the open areas, probably due to the building of campsites after disaster. As

seen in Table 4, by obtaining the ECDI for the two post-disaster images and then comparing them to the pre-disaster image, we were able to identify open spaces that were turned into campsites, then back to open spaces by the post T2 date, as well as the open spaces that remained as campsites by the post T2 date. With more post-disaster images, a progressive recovery can be observed.

The return of open spaces to their original state is an indication of normalcy and hence an important aspect of recovery monitoring over time. Areas in which open spaces stay occupied by camps for a long period of time indicate slow resettlement and development efforts as compared to the areas in which the campsites are cleared up. The location, size and relative change of the open spaces over time can be used by managers to better understand management practices pertaining to re-housing of the population and development efforts.

Table 4 Open Spaces Case Study Scenarios

This table notes scenarios that can be seen when enhanced change detection indices are observed over time.

ECDI of Pre disaster & Post T1*	ECDI of Pre disaster & Post T2*	ECDI of Post T1* & Post T2*	Scenario
>5	<5	>5	Open spaces occupied by camp site at Post T1* date and camp site removed by Post T2* date
>5	>5	<5	Open spaces occupied by camp site at Post T1* date and camp site still exists by Post T2* date
<5	<5	<5	Open spaces not occupied by camp sites
<5	>5	>5	Campsites not present at Post T1* date but campsites or development occurred at Post T2* date

*Post T1 and Post T2 are the dates that images were obtained after the disaster.

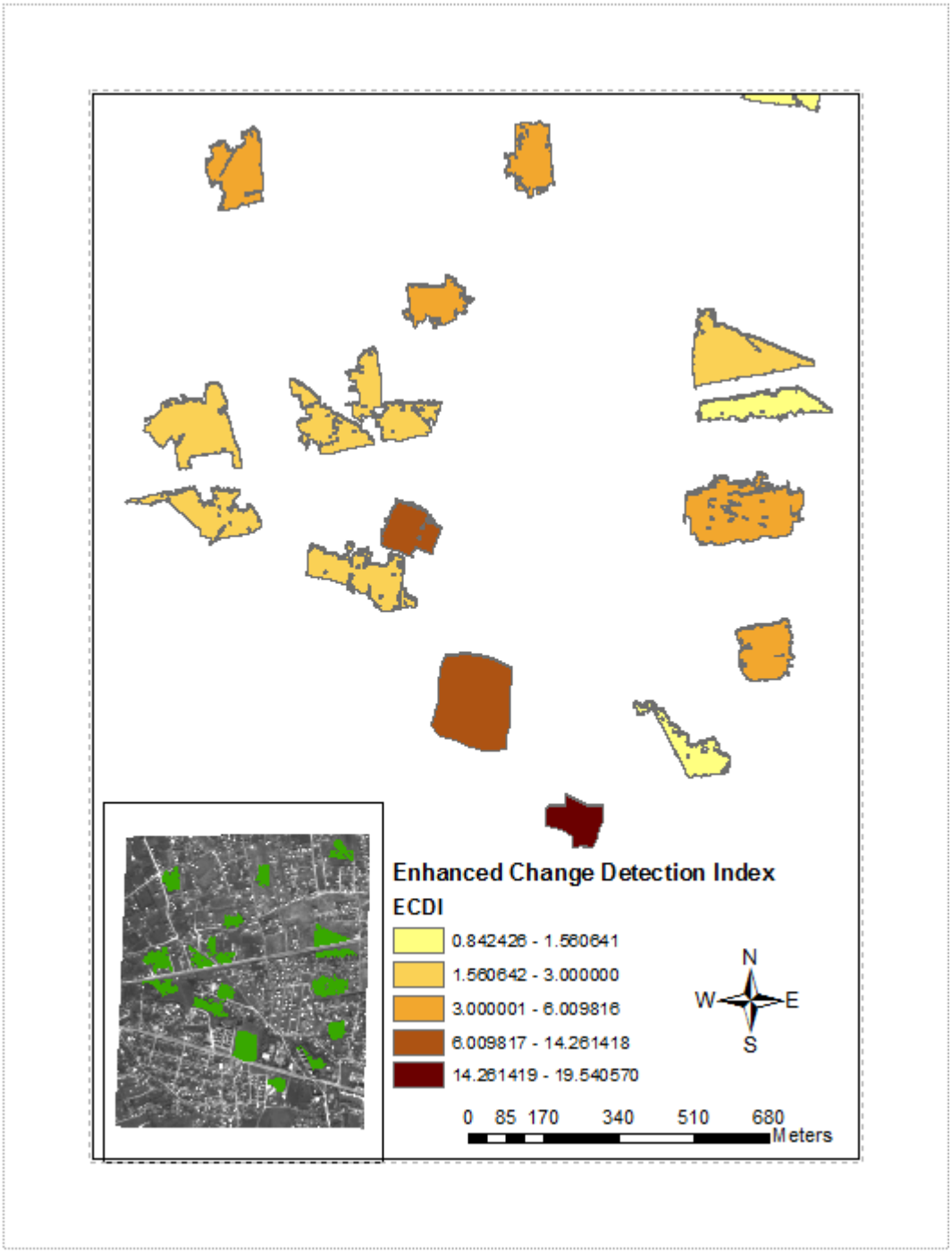

Figure 12: ECDI for the open areas of Van. Higher indices (represented by darker colors) indicate larger changes after the disaster.

4. Discussion and Conclusions

The proposed method uses indicators that pertain to recovery and monitoring as GIS objects and integrates existing knowledge into processing to optimize change detection. Each road class would have a specific texture, width, proximity to buildings, traffic, etc.; thus road types are compared with similar road types and bridges with similar bridges. In this study we separated primary roads from secondary roads. Provided one has more information about additional road categories, major and

minor roads within primary roads could be sub-categorized and analysed separately. This would also discriminate roads with heavy traffic from roads with less traffic, roads surrounded by trees from roads surrounded by buildings, and roads constructed of different materials, thereby increasing the accuracy.

This method uses the calculation of the texture, edges, and gradient of each object to better estimate the change between the pre- and post-disaster data. To determine what proportions of each of the above properties contribute to real change, a visual index is used to train the data. Like any user-derived parameter, the visual index can be very specific to the user. However, provided that the visual index is completed by a single user, it should contain relative differences representative of the changes within the image. It is easy to visually see objects that underwent a large change and those that experienced no change, so more objects at extremes were used for the visual index. It is best to use more objects at the ends of the change spectrum since the computer is then better able to estimate objects that are at different gradients of change.

The normalization between the pre- and post-disaster data reduces the differences caused due to the acquisition times and atmospheric anomalies of the pre/post images. The targeted change is relative to all roads in a particular road group. Thus the normalization specifically enhances the relative change, downplaying changes common to all roads in a particular road group. The VHR sensors used in this study collect data around the same time, so the shadow effect due to acquisition time will be minimal; the main issues are the incidence angle and changes in solar zenith, because these will impact the imagery more directly than the difference between acquisition times. The considered relative change by normalizing between the pre and post images would give more weight to the changes than the increase and decrease in shadows. During a non-rush hour the main roads will still have more vehicles than the alternative roads. Hence the vehicle changes due to the time of the day would not affect the analysis as this is a relative change normalized to all roads.

After a disaster, as seen in Figure 4 d) rubble and trees fallen on the road can be factors that cause change compared to the pre disaster image Figure 4 c). Rubble and fallen trees are brought out as a change easily in the pre/post normalization, unless the texture of the rubble mimics the texture created by vehicles in the same segment of the pre-disaster image. Most houses are not built close to highways, so rubble that resembles highly dense vehicle traffic is unlikely to affect the analysis. Rubble is primarily seen at the edges of the road and is visually different from the traffic seen in the two case studies; hence it was flagged as a change in both cases.

Once the change is quantified based on training data, the pre/post normalized method outlined in this paper can be used automatically to detect change and to observe recovery over time. Comparing the most recent image and consecutive past images can give a complete history of changes pertaining to

road segments. Another benefit is that this method can be used over large areas to get the big picture and determine changes over time.

The coefficients pertaining to the texture, edges, and gradient obtained from the visual index are transferable to other roads with similar construction material and thus similar reflective properties. This transferability works better for roads that are categorized to finer classes and are analysed separately. The same method can be applied to other categories such as bridges and railroads when analysed separately as a unique class of GIS objects. Buildings could also be analysed; this work has been completed and will be published as a follow-up. Applying this method of analysis over time is a significant advantage over analysis of ground truth data in temporal analysis. Analysis over time also contributes to the full picture of the recovery and development after disaster, thereby giving managers a tool to better understand management practices.

Acknowledgements This research was partly supported by the European Commission under FP7 (Seventh Framework Programme): "SENSUM: Framework to Intergrade Space-based and in-situ sENSing for dynamic vUlnerability and recovery Monitoring" (312972). We gratefully acknowledge the contribution from Enrica Verrucci and the anonymous referees.

References

Akcay, H.G., and S. Aksoy. 2008. 'Automatic Detection of Geospatial Objects Using Multiple Hierarchical Segmentations'. *IEEE Trans. Geosci. Remote Sensing* 46 (7): 2097-2111. doi:10.1109/tgrs.2008.916644.

Al-Khudhairy, D.H.A., I. Caravaggi, and S. Giada. 2005. "Structural Damage Assessments from Ikonos Data Using Change Detection, Object-Oriented Segmentation, And Classification Techniques". *Photogrammetric Engineering & Remote Sensing* 71 (7): 825-837. doi:10.14358/pers.71.7.825.

Blaschke, T. 2010. "Object Based Image Analysis For Remote Sensing". ISPRS Journal Of Photogrammetry And Remote Sensing 65 (1): 2-16. doi:10.1016/j.isprsjprs.2009.06.004.

Bouziani, Mourad, Kalifa Goita, and Dong-Chen He. 2010. 'Automatic Change Detection of Buildings in Urban Environment from Very High Spatial Resolution Images Using Existing Geodatabase and Prior Knowledge'. *ISPRS Journal of Photogrammetry And Remote Sensing* 65 (1): 143-153. doi:10.1016/j.isprsjprs.2009.10.002.

Brown, D., Bevington, J., Platt, S., Saito, K., Adams, B. J., Chenvidyakarn, T., Spence, R. J., Chuenpagdee, R., Khan, A., So, E., (2012) "Monitoring and Evaluating Post-Disaster Recovery Using High-Resolution Satellite Imagery – Towards Standardised Indicators

460 for Post-Disaster Recovery", ReBuilDD Workshop, Cambridge, UK.
461 Butenuth, Matthias, and Christian Heipke. 2010. 'Network Snakes: Graph-Based Object
462 Delineation with Active Contour Models'. *Machine Vision and Applications* 23 (1): 91-
463 109. doi:10.1007/s00138-010-0294-8.
464 Dai, X and S. Khorram. 1998. 'The Effects of Image Misregistration on the Accuracy of
465 Remotely Sensed Change Detection'. *IEEE Trans. Geosci. Remote Sensing* 36 (5): 1566-
466 1577. doi:10.1109/36.718860.
467 Dell'Acqua F, Lisini G, Gamba P 2009. 'Experiences in Optical and SAR Imagery
468 Analysis for Damage Assessment in the Wuhan, May 2008 Earthquake'. *In:*
469 *Proceedings of IGARSS 2009, Cape Town, South Africa, 13–17 July 2009.*
470 Download.geofabrik.de,.2015. http://download.geofabrik.de/europe/turkey.html.
471 Earthquake.usgs.gov,. 2005. 'PAKISTAN'.
472 http://earthquake.usgs.gov/earthquakes/eqinthenews/2005/usdyae/#details.
473 Earthquake.usgs.gov,. 2011. 'EASTERN TURKEY: Van'.
474 http://earthquake.usgs.gov/earthquakes/eqinthenews/2011/usb0006bqc/.
475 Gueguen L, Soille P, Pesaresi M (2011) 'Change Detection based on Information Measure.'
476 *IEEE Trans Geosci Remote Sens* 49(11):4503–4515
477 Kodge, B. G., Hiremath, P. S. (2011) 'Automatic Open Space Area Extraction and Change
478 Detection from High Resolution Urban Satellite Images. CoRR abs/1103.4913 (2011)
479 Lin, Chungan, and Ramakant Nevatia. 1998. 'Building Detection and Description from a
480 Single Intensity Image'. *Computer Vision And Image Understanding* 72 (2): 101-121.
481 doi:10.1006/cviu.1998.0724.
482 Mena, J.B., and J.A. Malpica. 2005. 'An Automatic Method for Road Extraction in Rural and
483 Semi-Urban Areas Starting from High Resolution Satellite Imagery'. *Pattern*
484 *Recognition Letters* 26 (9): 1201-1220. doi:10.1016/j.patrec.2004.11.005.
485 Michaelsen, Eckart, Uwe Soergel, and Ulrich Thoennessen. 2006. 'Perceptual Grouping for
486 Automatic Detection of Man-Made Structures in High-Resolution SAR Data'. *Pattern*
487 *Recognition Letters* 27 (4): 218-225. doi:10.1016/j.patrec.2005.08.002.
488 Mohammadzadeh, A., M. J. ValadanZoej, and A. Tavakoli. 2009. 'Automatic Main Road
489 Extraction from High Resolution Satellite Imageries by Means of Particle Swarm
490 Optimization Applied to a Fuzzy-Based Mean Calculation Approach'. *Journal of the*
491 *Indian Society of Remote Sensing* 37 (2): 173-184. doi:10.1007/s12524-009-0021-y.
492 Mohammadzadeh, A., M.J. ValadanZoej, and A. Tavakoli. 2008. 'Automatic Main Road

493 Extraction from High Resolution Satellite Imageries by Means of Self-Learning Fuzzy-
494 GA Algorithm'. *Journal of Applied Sciences* 8 (19): 3431-3438.
495 doi:10.3923/jas.2008.3431.3438.
496 Pagot, E., M. Pesaresi, D. Buda, and D. Ehrlich. 2008. 'Development of an Object-oriented
497 Classification Model Using Very High Resolution Satellite Imagery for Monitoring
498 Diamond Mining Activity'. *International Journal of Remote Sensing* 29 (2): 499-512.
499 doi:10.1080/01431160601047771.
500 QGIS Development Team, 2015. QGIS Geographic Information System Developers Manual.
501 Open Source Geospatial Foundation Project. Electronic document:
502 http://www.qgis.org/wiki/Developers_Manual
503 Singh, P. P., and R. D. Garg. 2014. 'Road Detection from Remote Sensing Images Using
504 Impervious Surface Characteristics: Review and Implication'. *Int. Arch. Photogramm.*
505 *Remote Sens. Spatial Inf. Sci.* XL-8: 955-959. doi:10.5194/isprsarchives-xl-8-955-2014.
506 Talib, Muhamad Lazim, and SuzaimahRamli. 2015. 'A Review of Multiple Edge Detection in
507 Road Lane Detection Using Improved Hough Transform'. *AMR* 1125: 541-545.
508 doi:10.4028/www.scientific.net/amr.1125.541.
509 Touya, Guillaume. 2010. 'A Road Network Selection Process Based on Data Enrichment And
510 Structure Detection'. *Transactions In GIS* 14 (5): 595-614. doi:10.1111/j.1467-
511 9671.2010.01215.x.
512 VictorDevadoss, A., and S.M.A. Shahul Hameed. 2015. 'Analyzing the Behavioral Changes
513 of Road User through Euclidean Distance Intuitionistic Fuzzy Valued Associative
514 Memories'. *International Journal of Computer Applications* 118 (10): 23-27.
515 doi:10.5120/20782-3416.
516 Vu, T. T., and Y. Ban. 2010. 'Context-Based Mapping of Damaged Buildings from High-
517 Resolution Optical Satellite Images'. *International Journal of Remote Sensing* 31 (13):
518 3411-3425. doi:10.1080/01431161003727697.
519 Walter, Volker. 2004. 'Object-Based Classification of Remote Sensing Data for Change
520 Detection'. *ISPRS Journal Of Photogrammetry And Remote Sensing* 58 (3-4): 225-238.
521 doi:10.1016/j.isprsjprs.2003.09.007.
522 Yang, J., and R. S. Wang. 2007. 'Classified Road Detection from Satellite Images Based on
523 Perceptual Organization'. *International Journal of Remote Sensing* 28 (20): 4653-4669.
524 doi:10.1080/01431160701250382.
525